CHEMISTRY OF MATERIALS
Article

Chem. Mater. **2010,** *22,* 197–206 197
DOI:10.1021/cm902731u

Hydrogen Bond-Assisted Supramolecular Self-Assembly of Doubly Discotic Supermolecules Based on Porphyrin and Triphenylene

Jianjun Miao[†] and Lei Zhu*[,†,‡]

[†]*Polymer Program, Institute of Materials Science and Department of Chemical, Materials and Biomolecular Engineering, University of Connecticut, Storrs, Connecticut 06269-3136, and* [‡]*Department of Macromolecular Science and Engineering, Case Western Reserve University, Cleveland, Ohio 44106-7202*

Received September 2, 2009. Revised Manuscript Received October 30, 2009

Hydrogen bonding is a powerful driving force for the supramolecular self-assembly of discotic mesogens, and molecular shape also plays an important role in such systems. To study these effects, doubly discotic supermolecules have been synthesized by linking a *meso*-tetraphenylporphine-4,4′,4″,4‴-tetracarboxylic acid (Py) core with four triphenylenes (Tp) arms via either amide or ester bonds. The spacer length between the Py core and Tp disks was C6 and C10, and the alkyl arm length in the Tp disks was C5 and C12, respectively. Compared to the ester-linked $Py(Tp)_4$ supermolecules, the amide-linked samples exhibited rich crystalline and liquid-crystalline phases, suggesting that the intracolumnar hydrogen-bonding among trans amide bonds was the primary driving force for the self-assembly. X-ray diffraction (XRD) was used to understand the supramolecular self-assembly of the amide-linked $Py(Tp)_4$ doubly discotic supermolecules. When the spacer length was no shorter than or similar to the triphenylene alkyl arm length, a rectangular boardlike molecular shape was adopted and thus lamellar structures were obtained. When the spacer length was much shorter than the triphenylene alkyl arms, an ellipsoidal overall molecular shape resulted, and thus a regular columnar phase was obtained. From this study, we speculated that hydrogen-bond-induced microphase separation between moieties with different electron affinities in doubly discotic supermolecules may be useful for the practical applications of organic electronics.

Introduction

Columnar discotic liquid crystals, which consist of rigid polyaromatic cores surrounded by flexible arms, are an interesting class of functional materials potential for photovoltaic cells,[1−3] light-emitting diodes,[4−9] and field-effect transistors[10,11] because of the high charge-carrier mobility along their one-dimensional (1D) aromatic $\pi-\pi$ stacking.[1,12] Besides the advantages of low cost, ability to scale up, and tunable energy gap for organic photovoltaics over inorganic materials, columnar discotic liquid crystals have unique properties such as easy processing, self-healing, and lacking of defects.[13] To apply the columnar structure for 1D charge conduction, the area of π-orbital overlapping[14] and the intracolumnar distance[15] are key factors affecting the efficiency of charge carrier mobility. To increase the overlapping area of $\pi-\pi$ stacking, a large conjugated polyaromatic core is required, such as hexa-*peri*-hexabenzocoronene (HBC)[13,16,17] and its derivatives with a charger carrier mobility as high as 1 $cm^2\ V^{-1}\ s^{-1}$, which is comparable to that of graphite (3 $cm^2\ V^{-1}\ s^{-1}$).[16] For organic semiconductors, the interdisk distance usually ranges from 0.33 to 0.4 nm.[14,18−21] To decrease the interdisk distance and

*Corresponding author. E-mail: lxz121@case.edu. Tel: 216-368-5861.

(1) Schmidt-Mende, L.; Fechtenkotter, A.; Mullen, K.; Moons, E.; Friend, R. H.; MacKenzie, J. D. *Science* **2001**, *293*, 1119–1122.
(2) Nelson, J. *Science* **2001**, *293*, 1059–1060.
(3) Oukachmih, M.; Destruel, P.; Seguy, I.; Ablart, G.; Jolinat, P.; Archambeau, S.; Mabiala, M.; Fouet, S.; Bock, H. *Sol. Energy Mater. Sol. Cells* **2005**, *85*, 535–543.
(4) Meier, H. *Angew. Chem.* **1992**, *104*, 1425–1446. Meier, H. *Angew. Chem., Int. Ed.* **1992**, *31*, 1399–1420.
(5) Christ, T.; Glusen, B.; Greiner, A.; Kettner, A.; Sander, R.; Stumpflen, V.; Tsukruk, V.; Wendorff, J. H. *Adv. Mater.* **1997**, *9*, 48–52.
(6) Bacher, A.; Bleyl, I.; Erdelen, C. H. *Adv. Mater.* **1997**, *9*, 1031–1035.
(7) Seguy, I.; Destruel, P.; Bock, H. *Synth. Met.* **2000**, *111*, 15–18.
(8) Hertmanowski, R.; Martynski, T.; Stolarski, R.; Bauman, D. *Opto-Electron. Rev.* **2008**, *16*, 237–243.
(9) Saleh, M.; Park, Y. S.; Baumgarten, M.; Kim, J. J.; Mullen, K. *Macromol. Rapid Commun.* **2009**, *30*, 1279–1283.
(10) van de Craats, A. M.; Stutzmann, N.; Bunk, O.; Nielsen, M. M.; Watson, M.; Mullen, K.; Chanzy, H. D.; Sirringhaus, H.; Friend, R. H. *Adv. Mater.* **2003**, *15*, 495–499.
(11) Pisula, W.; Menon, A.; Stepputat, M.; Lieberwirth, I.; Kolb, U.; Tracz, A.; Sirringhaus, H.; Pakula, T.; Mullen, K. *Adv. Mater.* **2005**, *17*, 684–689.
(12) Adam, D.; Schuhmacher, P.; Simmerer, J.; Haussling, L.; Siemensmeyer, K.; Etzbach, K. H.; Ringsdorf, H.; Haarer, D. *Nature* **1994**, *371*, 141–143.
(13) Simpson, C. D.; Wu, J. S.; Watson, M. D.; Mullen, K. *J. Mater. Chem.* **2004**, *14*, 494–504.
(14) van de Craats, A. M.; Warman, J. M. *Adv. Mater.* **2001**, *13*, 130–133.
(15) Liu, C.; Bard, A. J. *Nature* **2002**, *418*, 162–164.
(16) van de Craats, A. M.; Warman, J. M.; Mullen, K.; Geerts, Y.; Brand, J. D. *Adv. Mater.* **1998**, *10*, 36–38.
(17) van de Craats, A. M.; Warman, J. M.; Fechtenkotter, A.; Brand, J. D.; Harbison, M. A.; Mullen, K. *Adv. Mater.* **1999**, *11*, 1469–1472.
(18) Zamir, S.; Poupko, R.; Luz, Z.; Huser, B.; Boeffel, C.; Zimmermann, H. *J. Am. Chem. Soc.* **1994**, *116*, 1973–1980.
(19) Ito, S.; Wehmeier, M.; Brand, J. D.; Kubel, C.; Epsch, R.; Rabe, J. P.; Mullen, K. *Chem.—Eur. J.* **2000**, *6*, 4327–4342.
(20) Pieterse, K.; van Hal, P. A.; Kleppinger, R.; Vekemans, J.; Janssen, R. A. J.; Meijer, E. W. *Chem. Mater.* **2001**, *13*, 2675–2679.
(21) Ichihara, M.; Suzuki, A.; Hatsusaka, K.; Ohta, K. *J. Porphyrins Phthalocyanines* **2007**, *11*, 503–512.

Published on Web 12/01/2009

stabilize the columnar structure, various noncovalent interactions have been utilized, including electrostatic interactions, hydrophobic−hydrophilic effects, metal coordination, and hydrogen bonding. For example, an interdisk distances of 0.329 nm was reported for a tricycloquinazoline core (0.329 nm)[22] and 0.326 nm for lutetium phthalocyanine dimers.[23] Ivanov et al. reported the smallest intracolumnar stacking distance (0.318−0.32 nm) and a mobility as high as 0.04−0.08 cm^2 V^{-1} s^{-1} in a hexaazatriphenylene with six amide groups at the peripheral positions of the discotic core,[24] and it was concluded that hydrogen bonding was responsible for the decreased interdisk distance.

Another advantage of large polyaromatic molecules in organic photovoltaic applications is their intercolumnar distance in a range of a few to 10 nm, which is considered to be the optimal distance for the exciton diffusion.[25,26] Therefore, there has been substantial interest in applying *p*−*n* dyad-type discotic molecules for heterojunction photovoltaics.[27−29] However, *p*- and *n*-dyad discotic molecules tend to form alternating stacks within a column because of strong charge-transfer interactions between *p*- and *n*-moieties.[30−33] Therefore, it is important to induce mesophase separation between the *p* and *n* columns for practical applications.[34] To achieve this, researchers have utilized various strategies: (1) solubility difference-induced microphase separation during solution processing,[1] (2) antagonistic interactions among side chains,[35] and (3) hydrogen bonding.

An elegant example of hydrogen-bond-induced columnar liquid crystals in an otherwise nonliquid crystalline discotic molecules is 1,3,5-benzenetrisamides.[36−39] A C_3-symmetry was observed within a column, where the 120° rotation between neighboring benzenetrisamide molecules was stabilized by intermolecular hydrogen bonding along the column direction. In addition, a sergeants-and-soldiers principle was presented by Meijer et al. in these systems.[40−42] Paraschiv et al. reported a series of 1,3,5-benzenetrisamide with three pendent hexaalkoxytriphenylene groups by varying the spacer length and the arm length of the triphenylenes.[43,44] In total, four columnar hexagonal phases were identified, where intermolecular hydrogen bonds connected the central benzene cores in such a way that the adjacent benzene cores rotated 120° apart, therefore leading to a helical orientation of the resulting columnar stacks. A high mobility of 0.23 cm^2 V^{-1} s^{-1} was found in one of those triphenylene benzenetrisamide samples,[44] although it did not show the ordered intracolumnar stacking peak at 0.35 nm. The high mobility might be a result of the chirality, which induced a more favorable overlap among the pendant triphenylenes.

In this research, we replace the benzene core with a rigid porphyrin core, which is linked via amide bonds to four triphenylenes. Because the porphyrin dimension is much larger than that of a benzene ring and the symmetry changes from 3-fold to 4-fold, an entirely different self-assembly via hydrogen-bonding is expected. We speculate that the porphyrin cores will be linked together via intermolecular hydrogen-bonding, resulting in microphase separated porphyrin and triphenylene columns. To the best of our knowledge, there has been limited work reported on large doubly discotic mesogens with different electron affinities, although six triphenylenes have been attached directly to a triphenylene core, which had a hexagonal columnar phase.[45,46]

Experimental Section

Materials. *meso*-Tetraphenylporphine-4,4′,4″,4‴-tetracarboxylic acid was purchased from Frontier Scientific Inc. (Logan, UT). Benzotriazol-1-yl-oxytripyrrolidinophosphonium hexafluorophosphate (PyBOP) and *N*,*N*-diisopropylethylamine were purchased from Aldrich. Triphenylene monoamines were synthesized according to literature with certain modifications.[43,44] All solvents were purchased from Fisher Scientific and used without further purification.

General Synthesis Procedure and Characterization for Samples 1−4. Twenty mg (0.025 mmol) of *meso*-tetraphenylporphine-4,4′,4″,4‴-tetracarboxylic acid was activated by

(22) Kumar, S.; Rao, D. S. S.; Prasad, S. K. *J. Mater. Chem.* **1999**, *9*, 2751–2754.
(23) van de Craats, A. M.; Warman, J. M.; Hasebe, H.; Naito, R.; Ohta, K. *J. Phys. Chem. B* **1997**, *101*, 9224–9232.
(24) Gearba, R. I.; Lehmann, M.; Levin, J.; Ivanov, D. A.; Koch, M. H. J.; Barbera, J.; Debije, M. G.; Piris, J.; Geerts, Y. H. *Adv. Mater.* **2003**, *15*, 1614–1618.
(25) Terao, Y.; Sasabe, H.; Adachi, C. *Appl. Phys. Lett.* **2007**, *90*, 103515.
(26) Gommans, H.; Schols, S.; Kadashchuk, A.; Heremans, P.; Meskers, S. C. J. *J. Phys. Chem. C* **2009**, *113*, 2974–2979.
(27) Tchebotareva, N.; Yin, X. M.; Watson, M. D.; Samori, P.; Rabe, J. P.; Mullen, K. *J. Am. Chem. Soc.* **2003**, *125*, 9734–9739.
(28) Wasserfallen, D.; Fischbach, I.; Chebotareva, N.; Kastler, M.; Pisula, W.; Jackel, F.; Watson, M. D.; Schnell, I.; Rabe, J. P.; Spiess, H. W.; Mullen, K. *Adv. Funct. Mater.* **2005**, *15*, 1585–1594.
(29) Samori, P.; Fechtenkotter, A.; Reuther, E.; Watson, M. D.; Severin, N.; Mullen, K.; Rabe, J. P. *Adv. Mater.* **2006**, *18*, 1317–1321.
(30) Janietz, D. *J. Mater. Chem.* **1998**, *8*, 265–274.
(31) Cooke, G.; Kaushal, N.; Boden, N.; Bushby, R. J.; Lu, Z.; Lozman, O. *Tetrahedron Lett.* **2000**, *41*, 7955–7959.
(32) Schultz, A.; Laschat, S.; Abbott, A. P.; Langner, M.; Reeve, T. B. *J. Chem. Soc., Perkin. Trans. 1* **2000**, 3356–3361.
(33) Mahlstedt, S.; Janietz, D.; Stracke, A.; Wendorff, J. H. *Chem. Commun.* **2000**, 15–16.
(34) Hoeben, F. J. M.; Jonkheijm, P.; Meijer, E. W.; Schenning, A. *Chem. Rev.* **2005**, *105*, 1491–1546.
(35) Benanti, T. L.; Saejueng, P.; Venkataraman, D. *Chem. Commun.* **2007**, 692–694.
(36) Matsunaga, Y.; Miyajima, N.; Nakayasu, Y.; Sakai, S.; Yonenaga, M. *Bull. Chem. Soc. Jpn.* **1988**, *61*, 207–210.
(37) Hanabusa, K.; Koto, C.; Kimura, M.; Shirai, H.; Kakehi, A. *Chem. Lett.* **1997**, 429–430.
(38) Bushey, M. L.; Hwang, A.; Stephens, P. W.; Nuckolls, C. *J. Am. Chem. Soc.* **2001**, *123*, 8157–8158.
(39) Bushey, M. L.; Hwang, A.; Stephens, P. W.; Nuckolls, C. *Angew. Chem., Int. Ed.* **2002**, *41*, 2828–2831.
(40) Palmans, A. R. A.; Vekemans, J.; Havinga, E. E.; Meijer, E. W. *Angew. Chem., Int. Ed.* **1997**, *36*, 2648–2651.
(41) van Gorp, J. J.; Vekemans, J.; Meijer, E. W. *J. Am. Chem. Soc.* **2002**, *124*, 14759–14769.
(42) Smulders, M. M. J.; Schenning, A.; Meijer, E. W. *J. Am. Chem. Soc.* **2008**, *130*, 606–611.
(43) Paraschiv, I.; Giesbers, M.; van Lagen, B.; Grozema, F. C.; Abellon, R. D.; Siebbeles, L. D. A.; Marcelis, A. T. M.; Zuilhof, H.; Sudholter, E. J. R. *Chem. Mater.* **2006**, *18*, 968–974.
(44) Paraschiv, I.; de Lange, K.; Giesbers, M.; van Lagen, B.; Grozema, F. C.; Abellon, R. D.; Siebbeles, L. D. A.; Sudholter, E. J. R.; Zuilhof, H.; Marcelis, A. T. M. *J. Mater. Chem.* **2008**, *18*, 5475–5481.
(45) Plesnivy, T.; Ringsdorf, H.; Schuhmacher, P.; Nuetz, U.; Diele, S. *Liq. Cryst.* **1995**, *18*, 185–90.
(46) Zelcer, A.; Donnio, B.; Bourgogne, C.; Cukiernik, F. D.; Guillon, D. *Chem. Mater.* **2007**, *19*, 1992–2006.

58 mg (0.11 mmol) of PyBOP and 1 drop of *N*,*N*-diisopropylethylamine in 5 mL of anhydrous *N*,*N*-dimethylformamide (DMF). The mixture solution was sonicated for 10 min at room temperature, followed by addition of 0.11 mmol (86 mg for **1**, 92 mg for **2**, 139 mg for **3**, and 146 mg for **4**, see chemical structures in Scheme 1) of the corresponding triphenylene monoamine. The reaction mixture was further sonicated at room temperature for 30 min. The completion of reaction was checked by thin layer chromatography (TLC) using 1% methanol in chloroform as the developing solvent. The reaction mixture was then poured into 20 mL of double-distilled water and extracted with 10 mL of chloroform three times. The combined organic fractions were washed with 20 mL of 1 N HCl, 20 mL of 0.9 N $NaHCO_3$, and 20 mL of brine, respectively, before drying over anhydrous $MgSO_4$. After filtration and removal of the solvent under a vacuum, the crude products were purified by column chromatography (silica gel, gradient hexane to chloroform/methanol 99.75:0.25). Purple solids were obtained with yields: 60.3% for **1**, 68.0% for **2**, 50.1% for **3**, and 50.3% for **4**. The purity of all amide-linked samples was confirmed by TLC and size-exclusion chromatography (SEC), and narrow unimodel peaks (polydispersity indices (PDI) < 1.02) were obtained (see Figure 1).

^{1}H NMR for **1**, δ ($CDCl_3$): 1.0−0.85 (60H, m, CH_3), 2.0−1.2 (152H, m, CH_2 in alkyl tails), 3.58 (8H, m, CH_2NHCO), 4.3−4.15 (48H, m, $ArOCH_2$), 6.55 (4H, m, *NH*CO), 7.82 (24H, m, triphenylene Tp-*H*), 8.4−8.1 (16H, m, porphyrin phenyl Φ-*H*), 8.95 (8H, s, porphyrin pyrrole Py-*H*). ^{13}C NMR for **1** ($CDCl_3$): 14.1, 22.7, 26.0, 27.0, 29.4, 29.5, 29.6, 29.7, 29.8, 29.9, 31.9, 40.3, 69.8, 107.5, 119.3, 123.6, 125.4, 134.6, 145.1, 149.0, 167.5. ^{1}H NMR for **2**, δ ($CDCl_3$): 1.0−0.85 (60H, m, CH_3), 2.0−1.2 (184H, m, CH_2 in alkyl tails), 3.62 (8H, m, CH_2NHCO), 4.3−4.15 (48H, m, $ArOCH_2$), 6.43 (4H, m, *NH*CO), 7.82 (24H, m, triphenylene Tp-*H*), 8.4−8.1 (16H, m, porphyrin phenyl Φ-*H*), 8.95 (8H, s, porphyrin pyrrole Py-*H*). ^{13}C NMR for **2** ($CDCl_3$): 14.1, 22.7, 26.0, 27.0, 29.4, 29.5, 29.6, 29.7, 29.8, 29.9, 31.9, 40.3, 69.8, 107.5, 119.3, 123.6, 125.4, 134.6, 145.1, 149.0, 167.5. ^{1}H NMR of **3**, δ ($CDCl_3$): 1.0−0.85 (60H, m,

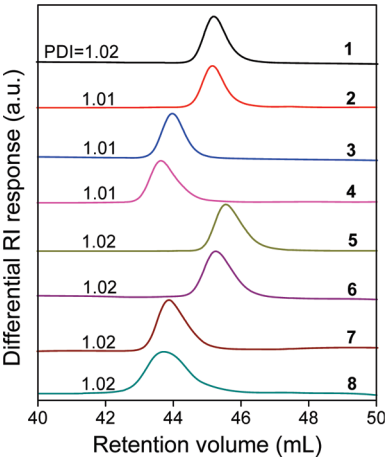

Figure 1. SEC differential refractive index (RI) curves for samples **1**−**8**. Polydispersity indices (PDI) are also shown for all the samples.

Scheme 1. Chemical Structure of Doubly Discotic Supermolecules Based on Porphyrin (Py) and Triphenylene (Tp), Py(Tp)$_4$, Linked by Amide or Ester Bonds

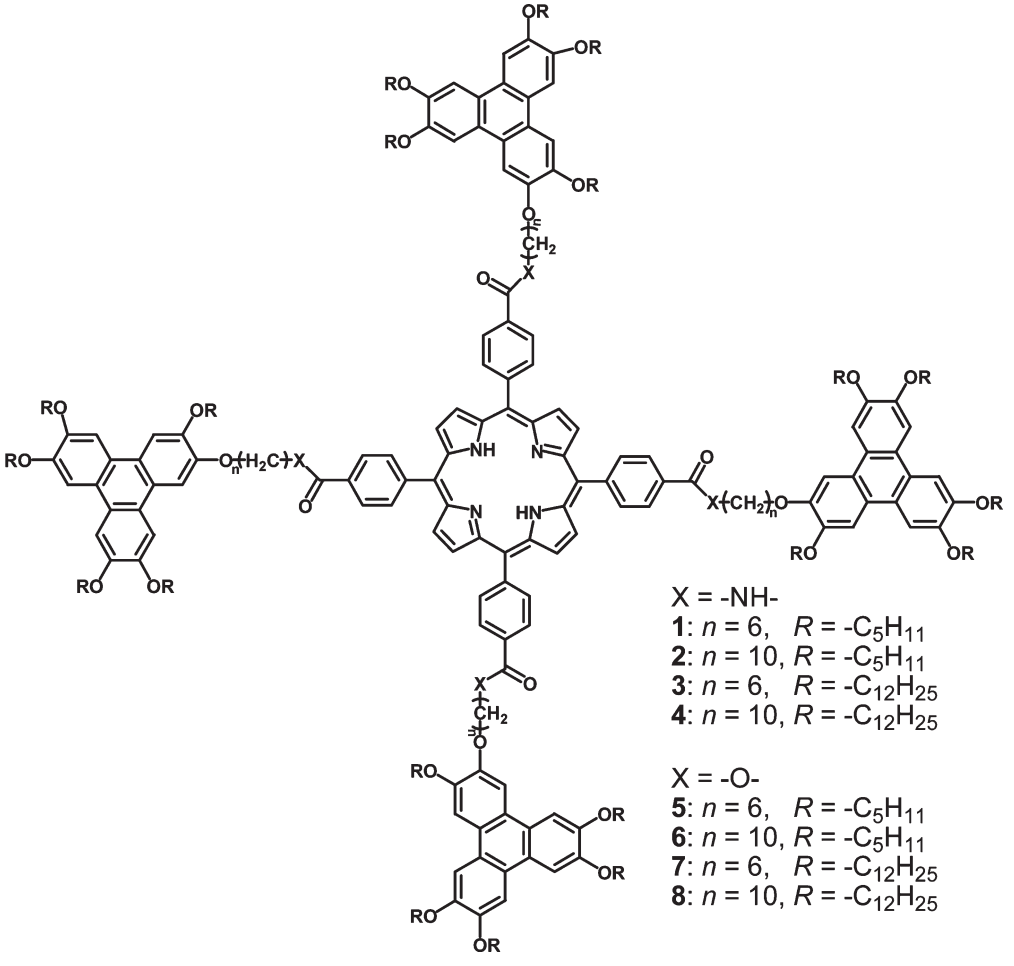

CH_3), 2.0−1.2 (432H, m, CH_2 alkyl tails), 3.61 (8H, m, CH_2NHCO), 4.3−4.15 (48H, m, ArOCH_2), 6.45 (4H, m, N*H*CO), 7.82 (24H, m, triphenylene Tp-*H*), 8.4−8.1 (16H, m, porphyrin phenyl Φ-*H*), 8.95 (8H, s, porphyrin pyrrole Py-*H*). ^{13}C NMR for **3** ($CDCl_3$): 14.1, 22.7, 26.0, 26.2, 27.0, 29.4, 29.5, 29.6, 29.7, 29.8, 29.9, 31.9, 40.3, 69.8, 107.5, 119.3, 123.6, 125.4, 134.6, 145.1, 149.0, 167.5. ^{1}H NMR of **4**, δ ($CDCl_3$): 1.0−0.85 (60H, m, CH_3), 2.0−1.2 (464H, m, CH_2 in alkyl tails), 3.61 (8H, m, CH_2NHCO), 4.3−4.15 (48H, m, ArOCH_2), 6.45 (4H, m, N*H*CO), 7.82 (24H, m, triphenylene Tp-*H*), 8.4−8.1 (16H, m, porphyrin phenyl Φ-*H*), 8.95 (8H, s, porphyrin pyrrole Py-*H*). ^{13}C NMR for **4** ($CDCl_3$): 14.1, 22.7, 26.0, 26.2, 27.0, 29.4, 29.5, 29.6, 29.7, 29.8, 29.9, 31.9, 40.3, 69.8, 107.5, 119.3, 123.6, 125.4, 134.6, 145.1, 149.0, 167.5.

General Synthesis Procedure and Characterization for Samples 5−8. 60 mg (0.35 mmol) of diethyl azodicarboxylate was slowly added to a suspension of 0.25 mmol of corresponding triphenylene alcohol (194 mg for **5**, 208 mg for **6**, 317 mg for **7**, and 331 mg for **8**), 50 mg (0.063 mmol) of *meso*-tetraphenylporphine-4,4′,4″,4‴-tetracarboxylic acid, and 85 mg (0.33 mmol) of triphenylphosphine in 10 mL of THF at room temperature. After the suspension had been sonicated for 30 min, 5 mL of chloroform, and 3 mL of water were added. The organic layer was extracted with water and brine, and dried over Na_2SO_4 before the solvent was removed. The residue was subject to a column chromatography (silica gel, using 50% hexane in chloroform as the eluent) and recrystallized from acetone to afford a purple solid. Yields: 46% for **5**, 44% for **6**, 51% for **7**, and 42% for **8**. The purity of all ester-linked samples was also confirmed by TLC and SEC, and narrow unimodel peaks (PDI = 1.02) were obtained (Figure 1).

^{1}H NMR for **5**, δ ($CDCl_3$): 1.0−0.85 (60H, m, CH_3), 2.0−1.2 (152H, m, CH_2 alkyl tails), 4.3−4.15 (48H, m, ArOCH_2), 4.6 (8H, m, COOCH_2), 7.82 (24H, m, triphenylene Tp-*H*), 8.6−8.3 (16H, m, porphyrin phenyl Φ-*H*), 8.85 (8H, s, porphyrin pyrrole Py-*H*). ^{13}C NMR for **5** ($CDCl_3$): 14.1, 22.7, 26.0, 27.0, 29.4, 29.5, 29.6, 29.7, 29.8, 29.9, 64.9, 69.8, 107.5, 119.3, 123.6, 125.4, 134.6, 145.1, 149.0, 166.0. ^{1}H NMR of **6**, δ ($CDCl_3$): 1.0−0.85 (60H, m, CH_3), 2.0−1.2 (184H, m, CH_2 alkyl tails), 4.3−4.15 (48H, m, ArOCH_2), 4.6 (8H, m, COOCH_2), 7.82 (24H, m, triphenylene Tp-*H*), 8.6−8.3 (16H, m, porphyrin phenyl Φ-*H*), 8.85 (8H, s, porphyrin pyrrole Py-*H*). ^{13}C NMR for **6** ($CDCl_3$): 14.1, 22.7, 26.0, 27.0, 29.4, 29.5, 29.6, 29.7, 29.8, 29.9, 64.9, 69.8, 107.5, 119.3, 123.6, 125.4, 134.6, 145.1, 149.0, 166.0. ^{1}H NMR of **7**, δ ($CDCl_3$): 1.0−0.85 (60H, m, CH_3), 2.0−1.2 (432H, m, CH_2 alkyl tails), 4.3−4.15 (48H, m, ArOCH_2), 4.6 (8H, m, COOCH_2), 7.82 (24H, m, triphenylene Tp-*H*), 8.6−8.3 (16H, m, porphyrin phenyl Φ-*H*), 8.85 (8H, s, porphyrin pyrrole Py-*H*). ^{13}C NMR for **7** ($CDCl_3$): 14.1, 22.7, 26.0, 26.2, 27.0, 29.4, 29.5, 29.6, 29.7, 29.8, 29.9, 64.9, 69.8, 107.5, 119.3, 123.6, 125.4, 134.6, 145.1, 149.0, 166.1. ^{1}H NMR of **8**, δ ($CDCl_3$): 1.0−0.85 (60H, m, CH_3), 2.0−1.2 (464H, m, CH_2 alkyl tails), 4.3−4.15 (48H, m, ArOCH_2), 4.6 (8H, m, COOCH_2), 7.82 (24H, m, triphenylene Tp-*H*), 8.6−8.3 (16H, m, porphyrin phenyl Φ-*H*), 8.85 (8H, s, porphyrin pyrrole Py-*H*). ^{13}C NMR for **8** ($CDCl_3$): 14.1, 22.7, 26.0, 26.2, 27.0, 29.4, 29.5, 29.6, 29.7, 29.8, 29.9, 64.9, 69.8, 107.5, 119.3, 123.6, 125.4, 134.6, 145.1, 149.0, 166.1.

Instrumentation and Characterization. ^{1}H NMR spectra were recorded on a Bruker spectrometer (500 MHz, DMX 500). Differential scanning calorimetry (DSC) experiments were carried out on a TA DSC-Q100 instrument. An indium standard was used for both temperature and enthalpy calibration. Approximately, 1−3 mg sample was used for the DSC study and the scanning rate was 10 °C/min. SEC was performed on a Viscotek GPCmax VE2001 with quadruple detectors. THF was used as the solvent and polystyrene standards were used for calibration. Polarized light microscopy (PLM) experiments were performed using an Olympus BX51P microscope equipped with an Instec HCS410 hot stage.

Two-dimensional (2D) X-ray diffraction (XRD) experiments were performed at the synchrotron X-ray beamline X27C at National Synchrotron Light Source (NSLS), Brookhaven National Laboratory (BNL). The wavelength of incident X-ray was 0.1371 nm. The scattering angle was calibrated using silver behenate with the primary reflection peak at the scattering vector $q = (4\pi\sin\theta)/\lambda = 1.076\ \mathrm{nm}^{-1}$, where θ is the half-scattering angle and λ is the wavelength. Fuji imaging plates were used as detectors for XRD experiments, and digital images were obtained using a Fuji BAS-2500 scanner. The typical data requisition time was 1 min. An Instec HCS410 hot stage equipped with a liquid-nitrogen cooling accessory was used for temperature-dependent X-ray experiments. One-dimensional (1D) XRD curves were obtained by integration of the corresponding 2D XRD patterns.

Results and Discussion

Hydrogen-Bond-Assisted Supramolecular Self-Assembly in Amide-Linked Samples 1−4. Supramolecular phase transitions in samples **1-4** were first studied by the DSC technique (Figure 2), and results are summarized in Table 1. Upon cooling, samples **1** and **2** showed single crystallization temperatures (T_c) at 173 (81.8 kJ/mol) and 144 °C (39.8 kJ/mol), respectively. Upon heating, they showed single melting temperatures (T_m) at 207 (83.6 kJ/mol) and 183 °C (39.8 kJ/mol), respectively. With increasing the spacer length from C_6 to C_{10}, the crystal melting temperature decreased by 24 °C. In addition, the sample **2** showed a glass transition temperature (T_g) at 74 °C upon heating. Judging from the heats of fusion and hysteresis in crystallization and melting temperatures ($\Delta T = T_m - T_c \approx 34-39$ °C) for both samples, they should have a crystalline phase below their T_m. However, in the PLM textures for samples **1** and **2** in images A and B in Figure 3, respectively, no typical spherulitic crystalline morphology was observed. Instead, a liquid-crystal-like texture was observed.

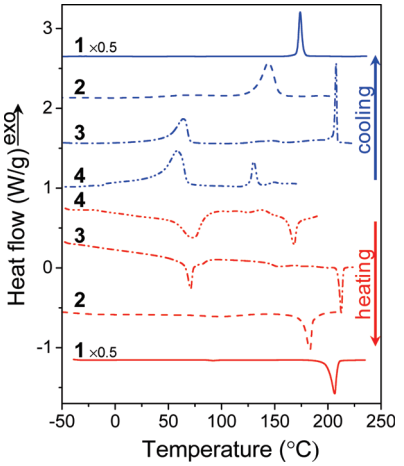

Figure 2. DSC first cooling and second heating curves for samples **1**−**4**. The scanning rate is 10 °C/min.

Table 1. Peak Phase Transition Temperatures (°C, above the arrow) and Heats of Transition (kJ/mol, below the arrow) for Samples 1−8[a]

sample	first cooling	second heating
1	$I \xrightarrow[81.8]{173} Cr(Py) + Col(Tp)$	$Cr(Py) + Col(Tp) \xrightarrow[83.6]{207} I$
2	$I \xrightarrow[39.8]{144} Cr(Py) + Col(Tp) \xrightarrow{54} g$	$g \xrightarrow{74} Cr(Py) + Col(Tp) \xrightarrow[39.8]{183} I$
3	$I \xrightarrow[71.9]{208} Col_o \xrightarrow[16.7]{147} Cr_1(Py) + LC(Tp) \xrightarrow[150]{64} Cr_2(Py + Tp)$	$Cr_2(Py + Tp) \xrightarrow[142]{71} Cr_1(Py) + LC(Tp) \xrightarrow[16.1]{152} Col_o \xrightarrow[70.8]{213} I$
4	$I \xrightarrow[19.6]{129} Col_L \xrightarrow[110]{58} Cr(Py + Tp)$	$Cr(Py + Tp) \xrightarrow[110]{74} Col_L \xrightarrow[28.3]{169} I$
5	$I \xrightarrow{6.3} g$	$g \xrightarrow{20} I$
6	$I \xrightarrow{9.0} g$	$g \xrightarrow{15} I$
7	$I \xrightarrow[85.3]{19} Cr(C_{12})$	$Cr(C_{12}) \xrightarrow[89.8]{37} I$
8	$I \xrightarrow[113.7]{20} Cr(C_{12})$	$Cr(C_{12}) \xrightarrow[119]{35} I$

[a] Cr = crystal; g = glass; LC = liquid crystal; Col = columnar phase; Col_L = lamello-columnar phase; I = isotropic; Py = porphyrin; Tp = triphenylene.

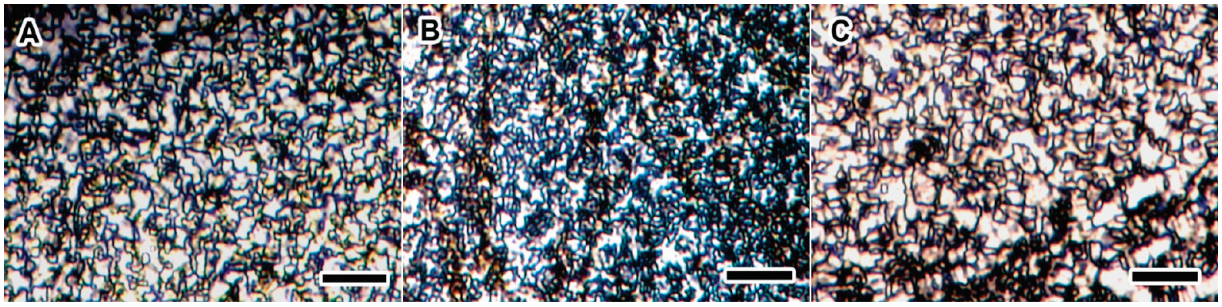

Figure 3. PLM micrographs for samples (A) **1**, (B) **2**, and (C) **4** at room temperature after slow cooling from the melt (scale bar is 15 μm for all images).

Unlike samples **1** and **2**, samples **3** and **4** exhibited multiple phase transitions upon cooling and heating, respectively (Figure 2). For example, upon cooling sample **3** showed a sharp peak at 208 °C (71.9 kJ/mol), a weak transition at 147 °C (16.7 kJ/mol), and a relatively broad peak at 64 °C (150 kJ/mol). Upon heating, three reverse processes took place at 71 (142 kJ/mol), 152 (16.1 kJ/mol), and 213 °C (70.8 kJ/mol), respectively. Judging from the heats of fusion and hysteresis between corresponding crystallization and melting peaks, the high-temperature (e.g., 175 °C) phase should be liquid crystalline and the low-temperature (e.g., 25 °C) phase should be crystalline. Detailed morphology and phase structures in the sample **3** will be discussed later. Upon cooling, the sample **4** shows a relatively sharp peak at 129 °C (19.6 kJ/mol) and a broad peak at 58 °C (110 kJ/mol). Upon heating, reverse processes are observed with a broad melting peak at 74 °C (110 kJ/mol) and a relatively sharp peak at 169 °C (28.3 kJ/mol). Again, judging from the magnitude of the heat of transition, the low temperature (e.g., 25 °C) phase should be a crystalline phase. However, the PLM texture of the sample **4** at room temperature in Figure 3C again showed a liquid-crystalline-like texture, which was similar to those of samples **1** and **2**.

Judging from the rich phase transitions in amide-linked samples **1**−**4**, we speculate that hydrogen-bonding is responsible for their supramolecular self-assembly behaviors. If the amide bonds in samples **1**−**4** are replaced by the ester linkages such as in samples **5**−**8**, no rich phase transitions were observed as evidenced in the DSC study in Figure 4. First, only a T_g around 17−20 °C was observed for samples **5** and **6**. Second, samples **7** and **8** showed a

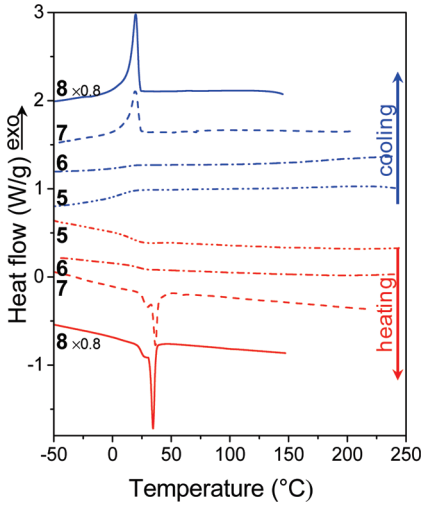

Figure 4. DSC first cooling and second heating curves for samples **5**−**8**. The scanning rate is 10 °C/min.

sharp T_m around 35 °C and a sharp T_c around 20 °C, respectively. The sharp low temperature transitions for samples **7** and **8** could be attributed to the C12 alkyl chain crystal melt and crystallization processes. Similar results were also observed in other C12 alkyl chain-containing liquid crystals reported before.[47,48] However, ordered

(47) Xue, C.; Jin, S.; Weng, X.; Ge, J. J.; Shen, Z.; Shen, H.; Graham, M. J.; Jeong, K. U.; Huang, H.; Zhang, D.; Guo, M.; Harris, F. W.; Cheng, S. Z. D.; Li, C. Y.; Zhu, L. *Chem. Mater.* **2004**, *16*, 1014–1025.
(48) Shen, H.; Jeong, K. U.; Xiong, H.; Graham, M. J.; Leng, S.; Zheng, J. X.; Huang, H.; Guo, M.; Harris, F. W.; Cheng, S. Z. D. *Soft Matter* **2006**, *2*, 232–242.

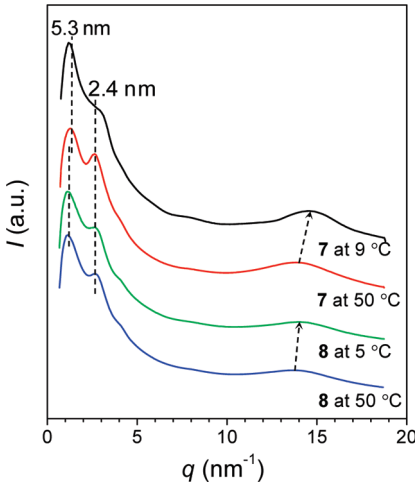

Figure 5. 1D XRD profiles for samples **7** and **8** after cooling from the melt to 9 and 5 °C, respectively.

C12 alkyl chains did not direct the ester-linked supermolecules to self-assemble into order structures as evidenced by the fact that nearly no (or very weak) birefringence was observed after cooling to 0 °C under PLM. This is further evidenced by temperature-dependent 1D XRD results in Figure 5. In the molten state at 50 °C, three broad peaks were observed at q = 1.12−1.25, 2.62, and 13.8 nm^{-1}, respectively. The peak at 1.12−1.25 nm^{-1} corresponded to a d-spacing of 5.6−5.3 nm, which could be attributed to the average distance among the porphyrin cores when the planar molecular size (ca. 6.8 nm) was considered. The peak at 2.62 nm^{-1} had a d-spacing of 2.4 nm, which could be attributed to the average distance among C12-triphenylenes. Finally, the amorphous halo at 13.7−13.8 nm^{-1} (~0.46 nm) represented the average distance among the alkyl chains. After the temperature decreased to 9 or 5 °C, the amorphous halos for **7** and **8** shifted to 14.5 and 13.9 nm^{-1}, respectively, and the peak at 1.12−1.25 nm^{-1} became slightly sharper. The slight shift in amorphous halos to higher q values after alkyl arm crystallization indicated certain ordering in the alkyl chains, which is similarly observed for low-ordered (e.g., nematic) liquid crystals.[49] Comparing the shift amount in q for samples **7** and **8**, the alkyl chains in **7** should have a higher order than those in the sample **8**.

Further evidence for hydrogen-bond-assisted supramolecular self-assembly in amide-linked $Py(Tp)_4$ supermolecules is demonstrated using a temperature dependent FTIR study. Typical results are shown in Figure 6 for the sample **3**, which showed an onset isotropization temperature at 208 °C. Below 206 °C, hydrogen-bonded N−H stretching and amide I C=O stretching absorption bands were observed at 3303 and 1640 cm^{-1}, respectively. The appearance of amide I band at 1640 cm^{-1} was consistent with a trans amide conformation.[47,50] Above

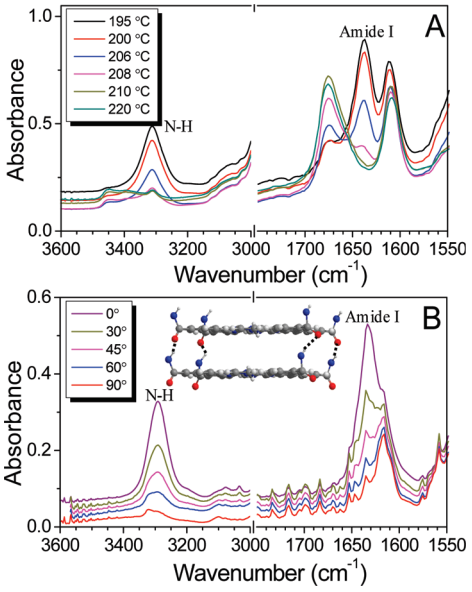

Figure 6. (A) Temperature-dependent FTIR spectra for the sample **3**. (B) Angle-dependent polarized light FTIR spectra for the oriented sample **3** with the polarized light angle changing from parallel (0°) to perpendicular (90°) with respect to the shear direction. Curves are offset for clarity.

208 °C, the intensity of hydrogen-bonded N−H and amide I bands substantially decreased in intensity. Meanwhile, broad new absorption bands appeared at 3434 and 1672 cm^{-1}, which could be assigned to non-hydrogen-bonded N−H and amide C=O absorption bands. Similar results were also seen for samples **1**, **2**, and **4** (see Figure S1 in the Supporting Information). We therefore conclude that hydrogen bonding is the primary driving force for the supramolecular self-assembly of samples **1**−**4** below the isotropization/melting temperature. The low-temperature transition at 71 °C for the sample **3** could be attributed to the partial ordering of C_{12} alkyl chains as well as the whole molecule crystallization. At room temperature (below 71 °C), the C_{12} alkyl chains had a significant amount of the trans conformation, as evidenced by a relatively strong 2850 cm^{-1} CH_2 asymmetric stretching band in FTIR, whereas above 100 °C, the band shift to 2854 cm^{-1} indicating substantially decreased amount of the trans conformation.[47] Similar result was also found for the sample **4** (see Figure S2 in the Supporting Information). Judging from the breath of the low-temperature transition and its heat of fusion, we conclude that the broad low temperature transitions upon heating for samples **3** and **4** should be combined melting processes of partially ordered alkyl chains and molecular crystals. This is different from the sharp melting peaks of C_{12} alkyl chain crystals in samples **7** and **8**.

The direction of hydrogen-bonding in the sample **3** was studied by polarized FTIR at room temperature, and the results are shown in Figure 6B. The 0° angle was defined as the polarization plane parallel to the shear direction. Presumably, after mechanical shear, the $\pi-\pi$ stacking (or the column) direction conformed to the shear direction for columnar liquid crystals (note that shearing was performed in the liquid crystalline phase at 164 °C). Obviously, the amide I and the N−H absorption bands

(49) Ruan, J. J.; Jin, S.; Ge, J. J.; Jeong, K. U.; Graham, M. J.; Zhang, D.; Harris, F. W.; Lotz, B.; Cheng, S. Z. D. *Polymer* **2006**, *47*, 4182–4193.
(50) Schneider, J.; Messerschmidt, C.; Schulz, A.; Gnade, M.; Schade, B.; Luger, P.; Bombicz, P.; Hubert, V.; Fuhrhop, J. H. *Langmuir* **2000**, *16*, 8575–8584.

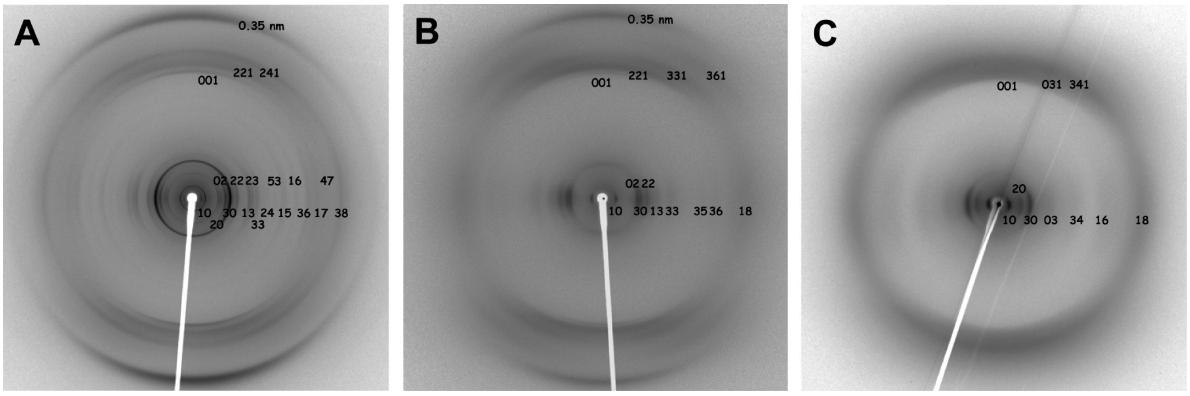

Figure 7. 2D XRD patterns for samples (A) **1**, (B) **2**, and (C) **4** at room temperature. All samples show an orthorhombic symmetry and Miller indices for all reflections are shown in the patterns. Because of the space limitation, all (*hk0*) reflections are shown as (*hk*) on the equator.

at 1640 and 3300 cm^{-1} were the strongest when the angle was 0° and the weakest when the angle was 90°, suggesting that the hydrogen bonds were along the $\pi-\pi$ stacking (or column) direction. Similar results were also observed for samples **1**, **2**, and **4** (data not shown here).

Hydrogen Bond-Assisted Lamellar Supramolecular Structures in Samples 1, 2, and 4. On the basis of the above DSC results, samples **1**, **2**, and **4** should have a crystalline phase at room temperature. To solve their structures, 2D XRD experiments were performed on shear-oriented samples and the shear temperatures were chosen at a few to 20 °C below the T_m. All the 2D XRD patterns in Figure 7 can be explained by an orthorhombic symmetry, and the assigned Miller indices are also shown in Figure 7 (assignments for samples **1**, **2**, and **4**, see Tables S1−S3 in the Supporting Information). Judging from the distinct (100), (200) (extinct for samples **2** and **4**), and (300) reflections in the 2D XRD patterns, a lamellar microstructure must be formed in the bulk samples. The unit-cell dimensions are determined as: $a = 4.82$ nm, $b = 3.50$ nm, and $c = 0.49$ nm for the sample **1**; $a = 4.89$ nm, $b = 3.50$ nm, and $c = 0.49$ nm for the sample **2**; $a = 5.78$ nm, $b = 3.50$ nm, and $c = 0.49$ nm for the sample **4**.

However, the outermost reflection with a *d*-spacing of 0.35 nm located in between the first and second layers of the [00*L*]-uniaxial XRD patterns for samples **1** and **2** in patterns A and B in Figure 7, respectively. Apparently, this reflection did not belong to the crystalline structure determined above, but is typical from the $\pi-\pi$ stacking in ordered triphenylene-based columnar liquid crystals.[51] Therefore, these XRD results indicate that the porphyrin cores and the triphenylene arms must microphase separate into distinct phases at nanoscale; the porphyrin cores crystallized into a crystalline lamella because of intermolecular hydrogen bonding along the trans amide linkages, whereas the triphenylenes formed an ordered columnar liquid-crystalline phase sandwiched between neighboring porphyrin lamellar crystals. For the sample **4**, no 0.35 nm spacing was observed in Figure 7C, suggesting that the triphenylenes might form a disordered columnar phase

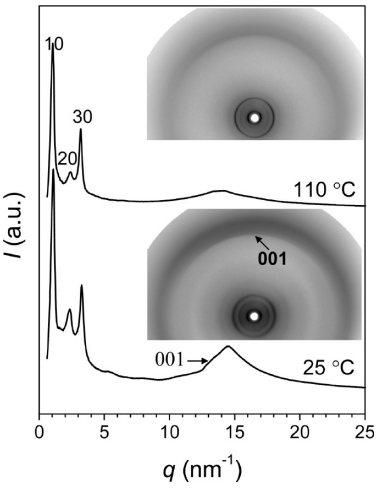

Figure 8. 1D XRD profiles and corresponding 2D XRD patterns at 110 and 25 °C for the sample **4**.

sandwiched between neighboring porphyrin crystals. Nematic discotic phase was unlikely to exist because no diffuse nematic discotic reflection was observed at low angles, as reported before.[52]

After heating the sample **4** to 110 °C, the porphyrin and C_{12} alkyl crystals melted, as evidenced by the disappearance of the (001), (031), and (341) crystalline reflections in the wide-angle region in Figure 8. The remaining of the (100), (200), and (300) reflections in the low angle region indicated that a lamellar liquid crystalline phase was preserved at elevated temperatures, where no crystalline registry should exist among neighboring lamellae. Inferring from the FTIR result that hydrogen bonding still existed below the isotropization temperature at 169 °C (see Figure S1 in the Supporting Information), we speculate that the sample **4** should have a lamello-columnar liquid crystalline phase.

Taking into account of the molecular sizes for the porphyrin (side length of the square-shaped core = 1.42 nm) and triphenylene (core diameter = 0.9 nm) moieties, we propose a molecular packing model for the amide-linked $Py(Tp)_4$ supermolecules **1**, **2**, and **4** (see Figure 9). First, porphyrin and triphenylene moieties form a

(51) Wang, T.; Yan, D.; Luo, J.; Zhou, E.; Karthaus, O.; Ringsdorf, H. *Liq. Cryst.* **1997**, *23*, 869–878.

(52) Cui, L.; Miao, J.; Zhu, L.; Sics, I.; Hsiao, B. S. *Macromolecules* **2005**, *38*, 3386–3394.

microphase-separated lamellar nanostructure, where porphyrin is crystalline and triphenylene is liquid crystalline. Second, the square-shaped porphyrin cores are linked together via hydrogen bonds at the four corners into a 2D lamellar crystal and the triphenylene moieties form columnar liquid crystals with a double-layer structure due to the aromatic $\pi-\pi$ stacking (see the top and side views in panels A and B in Figure 9). Note that in the top-view packing scheme in Figure 9A, each porphyrin core only corresponds to two triphenylenes. The only way to arrange four triphenylenes covalently connected to a porphyrin core in a three-dimensional space is that the porphyrin cores have to stack with a staggered arrangement and the face-to-face distance (the *c*-axis) is determined experimentally as 0.49 nm, as shown in the side view in Figure 9C (or the rectangular unit cell viewed along the *a*-axis is face-centered). Using experimental unit-cell dimensions obtained from the above XRD studies, the density of the porphyrin lamella is around 1.07 g/cm^3. Third, triphenylenes form a double-layer ordered columnar liquid crystalline phase and the $\pi-\pi$ stacking distance is 0.35 nm. The crystalline registry between the adjacent lamellae should exist in the crystalline phases for samples **1**, **2**, and **4** at low temperatures, but should be lost in the lamello-columnar liquid crystalline phase for the sample **4** at high temperatures. Thus, a dashed line is used between two triphenylene layers to represent a possible glide plane in Figure 9A. When the arm length in triphenylenes increases such as in the sample **4**, the ordering within a column is lost and the reflection at 0.35 nm thus disappears. Using experimental unit-cell dimensions obtained from the above XRD studies, the density of the triphenylene double-layer lamellae is between 1.13 and 1.27 g/cm^3, dependent on the alkyl chain length. This is reasonable for triphenylene liquid crystals with C12 arms.

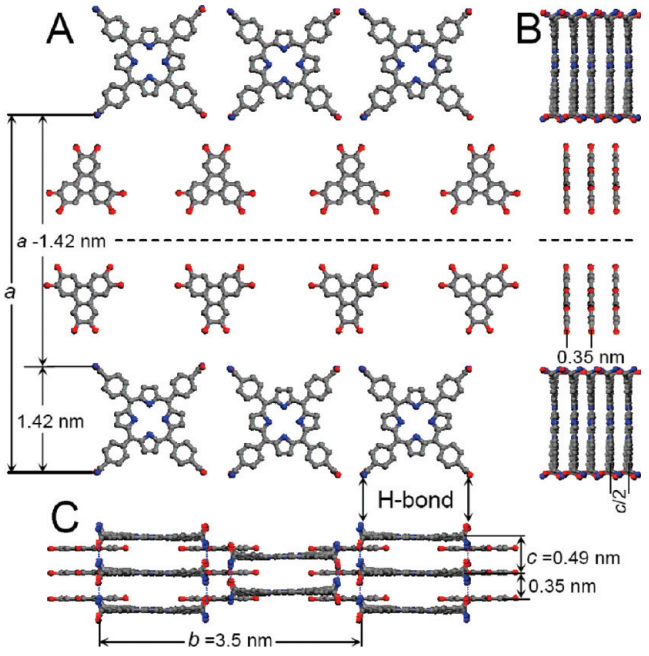

Figure 9. Schematic representation of self-assembled lamellar structures in Py(Tp)$_4$ supermolecules, **1**, **2**, and **4**, with amide linkages: (A) top view along the *c*-axis; (B) and (C) side views along the *a*- and *b*-axes, respectively. Note that alkyl arms and spacers are ignored for clarity, and dotted blue lines represent hydrogen bonds. The orthorhombic unit cell for porphyrin is represented by *a*, *b*, and *c*. Samples **1** and **2** had an ordered $\pi-\pi$ stacking distance of 0.35 nm for triphenylenes, whereas the sample **4** did not.

Hydrogen-Bond-Assisted Columnar Supramolecular Structure in Sample 3. Although the sample **3** showed a similar thermal behavior as that of the sample **4**, the PLM textures (see Figure 10) are drastically different from that of the sample **4** in Figure 3C. At 205 °C, a typical columnar liquid-crystalline texture is seen in Figure 10A.[47] After cooling to 150 °C, a fanlike texture is observed in Figure 10B. Finally, at room temperature, the texture does not change much from that at 150 °C. From these textures, we speculate that the high-temperature phase should be a columnar phase and the room-temperature phase should be a crystalline phase.

XRD was again utilized to investigate the hydrogen bond-assisted supramolecular self-assembly in the sample **3**. Figures 11 and 12 show 1D and 2D XRD profiles/patterns for the sample **3** at different temperatures during a stepwise cooling process from the melt. At 175 °C, all reflections in the 1D XRD profile can be fitted using an ordered oblique columnar (Col_o) unit cell with $a = 7.88$ nm, $b = 6.10$ nm, and $\gamma = 95°$ (see Table S4 in the Supporting Information). The corresponding 2D XRD pattern in Figure 12C showed all reflections on the equator, except for the 0.49 nm reflection on the meridian, which can be assigned as the ordered stacking distance between adjacent porphyrins via hydrogen bonding. The Miller indices close to the beam stop are shown in the magnified 2D image at the bottom of the figure. At 120 °C, the 1D XRD profile changed, and could be fitted with a monoclinic unit cell with $a = 8.03$ nm, $b = 5.50$ nm, $c = 0.49$ nm, and $\gamma = 95°$. The corresponding

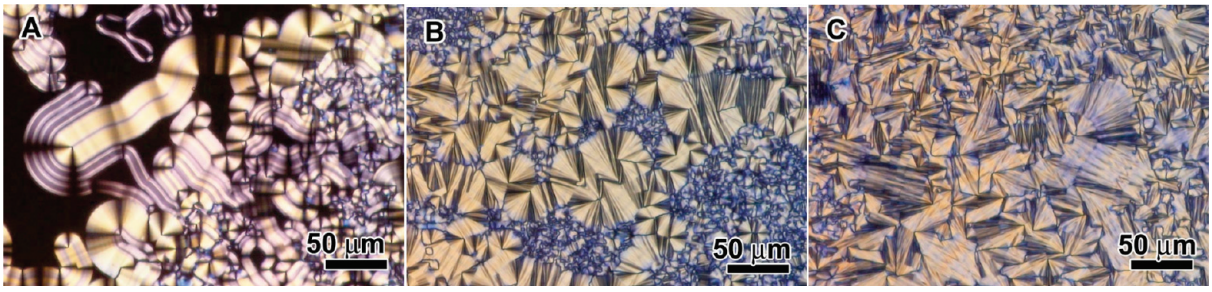

Figure 10. PLM micrographs for sample **3** at (A) 205, (B) 150, and (C) 25 °C, respectively, during slow cooling from the melt.

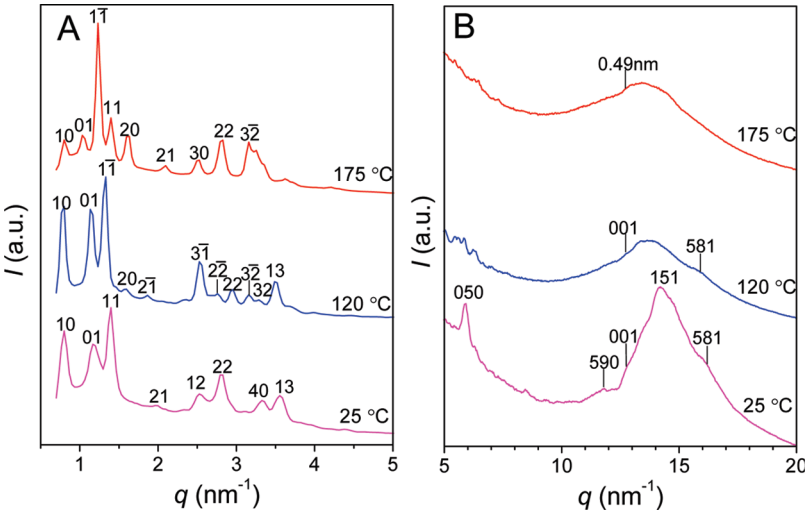

Figure 11. 1D (A) small- and (B) wide-angle XRD profiles for sample **3** at different temperatures during the second heating process.

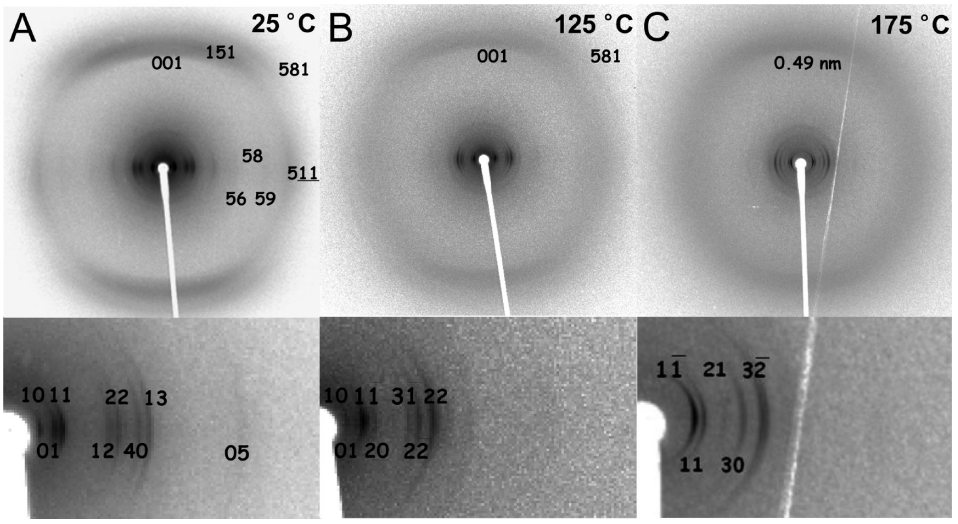

Figure 12. 2D XRD patterns for the sample **3** at (A) 25, (B) 125, and (C) 175 °C. Miller indices for reflections are shown in the patterns. Because of space limitations, all (*hk0*) reflections are shown as (*hk*) on the equator.

2D XRD pattern in Figure 12B showed reflections on both the equator and the first layer line, where the (151) and (581) reflections started to appear in the quadrant. At 25 °C, the 1D XRD profile further changed and could be fitted with an orthorhombic unit cell with $a = 7.82$ nm, $b = 5.37$ nm, and $c = 0.49$ nm. Again, the Miller indices are shown in the 2D images with broad reflections in the quadrant, suggesting that the registry among different layers was relatively poor. Similar to sample **4**, sample **3** did not show the ordered interdisk stacking distance between face-to-face triphenylenes at 0.35 nm.

Judging from the unit-cell dimensions, which are much larger than those for sample **4**, the supermolecule **3** should pack in a completely different structure than the high-temperature lamello-columnar phase in sample **4**, even though its spacer is shorter. Instead, sample **3** should form a regular columnar phase with whole molecules face-to-face stacking together to form a column (see Figure 13), because the whole molecule diameter was ca. 6.8 nm (two triphenylenes (2.4 nm) and one porphyrin (2.0 nm)). Because the intercolumnar distance for the

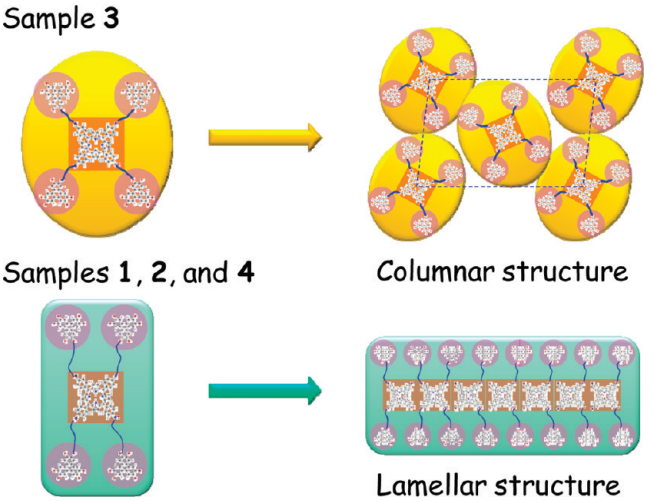

Figure 13. Molecular packing schemes for the samples **3** into a columnar structure and samples **1**, **2**, and **4** into a lamellar structure.

C_{12}-triphenylenes (2.4 nm) was observed at 2.6 nm^{-1} but the typical $\pi-\pi$ stacking distance (0.35 nm) was not observed for the sample **3**, we consider that the peripheral

triphenylenes formed a disordered columnar phase around the porphyrin column. At 175 °C, there was no registry along different porphyrin columns, resulting in an oblique columnar phase (see Figure 10A). Below 150 °C, registry started to develop along different porphyrin columns, forming a crystalline morphology (see Figure 10B). After being cooled to room temperature, both C12 arms in triphenylenes and the molecules started to crystallize, resulting in an orthorhombic crystal (see Figure 10C).

On the basis of the above results, we conclude that in addition to the hydrogen bonding, the relative length of the spacer with respect to the alkyl arms in triphenylenes also determines the supramolecular self-assembly of the amide-linked $Py(Tp)_4$ supermolecules. Only when the spacer is shorter than the alkyl chains, can the alkyl chain in the triphenylenes fill up the empty space between adjacent triphenylenes in a $Py(Tp)_4$ supermolecule. As a result, the whole supermolecule adopts an ellipsoid (or rounded) shape, which is able to self-assemble into a columnar liquid-crystalline phase (see the top panel in Figure 13). Otherwise (i.e., the spacer is similar to or longer than the alkyl arms in triphenylenes), the empty space between adjacent triphenylenes in a $Py(Tp)_4$ molecule cannot be filled, and thus the supermolecule will adopt a rectangular shape with two adjacent triphenylenes align together at one side and the other two at the other side of the porphyrin core during the hydrogen bond-assisted self-assembly. Consequently, a lamellocolumnar phase will be resulted (e.g., the sample **4** at 110 °C; see the bottom panel in Figure 13).

Conclusions

In summary, we designed a series of doubly discotic supermolecules with a 4-fold symmetry based on triphenylene and porphyrin connected via either amide or ester bonds. Comparing the experimental results between the amide- and ester-linked $Py(Tp)_4$ supermolecules, hydrogen bonding along the porphyrin columns was clearly responsible for the supramolecular self-assembly. Besides hydrogen bonding, the molecular shape was also an important determining factor for the supramolecular self-assembly of $Py(Tp)_4$. For samples **1**, **2**, and **4**, the spacer length was no shorter than or similar to the triphenylene alkyl arm lengths, and a rectangular planar shape was adopted. As a result, lamellar structures were resulted. For the sample **3**, the spacer was much shorter than the triphenylene alkyl arms, and an ellipsoid overall molecular shape was resulted. Consequently, a regular columnar phase was obtained. We speculated that the microphase separated porphyrin and triphenylene columns might be useful for organic photovoltaic and photochemical applications.

Acknowledgment. This work was supported by NSF CAREER Award DMR-0348724, DuPont Young Professor Grant, and 3M Nontenured Faculty Award. The synchrotron X-ray experiments were carried out at the National Synchrotron Light Source, Brookhaven National Laboratory, supported by the U.S. Department of Energy. Assistance from Dr. Lixia Rong, Dr. Jie Zhu, and Prof. Benjamin Hsiao at State University of New York at Stony Brook for synchrotron X-ray experiments is acknowledged.

Supporting Information Available: Temperature-dependent FTIR spectra for samples **1**, **2**, and **4** showing N−H and amide I absorption bands; FTIR spectra of samples **3** and **4** at different temperatures showing CH_2 asymmetric stretching bands; observed and calculated *d*-spacings for different reflections for samples **1**−**4** (PDF). This material is available free of charge via the Internet at http://pubs.acs.org.